Langmuir
Article
pubs.acs.org/Langmuir
© 2009 American Chemical Society

Aerosol-Based Self-Assembly of Nanoparticles into Solid or Hollow Mesospheres

Chunwei Wu,[†] Donggeun Lee,[‡] and Michael R. Zachariah*,[†]

[†]*Departments of Mechanical Engineering and Department of Chemistry and BioChemistry, University of Maryland, College Park, Maryland 20742, and* [‡]*School of Mechanical Engineering, Pusan Clean Coal Center, Pusan National University, Busan 609-735, South Korea*

Received September 10, 2009. Revised Manuscript Received October 29, 2009

The ability to manipulate miniature object assemblies with well-defined structures in a controllable manner is of both fundamental and applied interests. This article presents general strategies, with nanospheres as building blocks, to engineer mesoscopic spherical architectures via a process of evaporation-driven self-assembly in aerosol droplets. Uniform magnetite iron oxide (Fe_3O_4, ~2.5 nm), silica (SiO_2, ~15 nm), and cupric oxide (CuO, ~6 nm) nanoparticles were employed for the structural architecture. The method enables microstructural control of the self-assembled mesospheres by tuning the competition between solvent evaporation and solute diffusion within an aerosol droplet. Furthermore, we have demonstrated it is technically feasible to assemble surface-dissimilar binary components, i.e., charge-stabilized hydrophilic SiO_2 and hydrophobic ligand-capped Fe_3O_4 nanoparticles, into hierarchical composite structures, which could be extended for preparation of more hierarchically textured materials with desired functionalities.

Introduction

As opposed to the usual "top-down" manufacturing technique, nanofabrication approaches generally employ "bottom-up" assembly of a material's constituent units. Molecular or colloidal self-assembly is an important example of a "bottom-up" paradigm, from which well-defined patterns or superstructures on multiple length scales can be fabricated with a precision that challenges current lithographic techniques. Self-assembly is realized by spontaneous organization of molecular units into ordered structures as a result of local and weak interactions (e.g., van der Waals, electrostatics, $\pi-\pi$, hydrogen bonds, and capillary), in contrast to the more general strong interactions such as covalent, ionic, and metallic bonds, in order to maximize thermodynamic stability.[1,2]

Colloidal nano/meso spherical particles have been successfully utilized for constructing long-range ordered and periodic crystalline structures particularly on planar substrates. For example polystyrene latex or silica microspheres can be plated along a flat surface to create two-dimensional arrays and patterns,[3] structured coatings,[4] and porous structures with fine-tuned pore dimensions.[5] During the process of solvent evaporation, the crystallization of nanoparticles is driven by capillary forces.[6] Similarly, two- and three-dimensional superlattices have been observed on TEM grids as a result of the crystallization of monodisperse quantum dots (e.g., PbSe, PbTe, and CdSe)[7] or magnetic nanocrystals (e.g., Co and FePt)[8] after solvent evaporation.

Solvent evaporation is also capable of driving the self-assembly of surfactant micelles into periodic mesophases after exceeding the critical micelle concentration (cmc) and has been used extensively in conjunction with for example silicon alkoxides to prepare porous structures.[9] This approach has also been combined with an aerosol route to create a continuous production process of mesoporous powders or films.[10]

In this work we use an aerosol process to create self-assembled mesopsheres. The aerosol technique offers inherent benefits of maximizing the drying of solvent, and it restricts the self-assembly to take place within a micrometer-sized droplet, so that the derived mesospheres can be potentially used as building blocks for higher level self-ordering. More importantly, aerosol processes offers controllable solvent evaporation with respect to the diffusion of solute (i.e., nanospheres) and thus enables morphology and structural control of the assemblies. We demonstrate a generic aerosol process to assemble component nanoparticles such as Fe_3O_4, SiO_2, and CuO as well as binary primaries by employing a miscible trisolvent system. Such unique compact or hollow structures from the organization of building blocks has many promising applications including but not limited to photonic crystals,[11,12] catalysis,[11,13] and drug encapsulation/delivery.[11,14]

*Corresponding author. E-mail: mrz@umd.edu.

(1) Alder, B. J.; Hoover, W. G.; Young, D. A. *J. Chem. Phys.* **1968**, *49*, 3688.
(2) Shevchenko, E. V.; Talapin, D. V.; Kotov, N. A.; O'Brien, S.; Murray, C. B. *Nature* **2006**, *439*, 55.
(3) (a) Masuda, Y.; Itoh, T.; Koumoto, K. *Langmuir* **2005**, *21*, 4478. (b) Chen, X.; Sun, Z.; Zheng, L.; Chen, Z.; Wang, Y.; Fu, N.; Zhang, K.; Yan, Y.; Liu, H.; Jing, L.; Yang, B. *Adv. Mater.* **2004**, *16*, 1632.
(4) Prevo, B. G.; Kuncicky, D. M.; Velev, O. D. *Colloids Surf., A* **2007**, *311*, 2.
(5) (a) Velev, O. D.; Kaler, E. W. *Adv. Mater.* **2000**, *12*, 531. (b) Velev, O. D.; Lenhoff, A. M. *Curr. Opin. Colloid Interface Sci.* **2000**, *5*, 56.
(6) Danov, K. D.; Kralchevsky, P. A.; Boneva, M. P. *Langmuir* **2004**, *20*, 6139.
(7) (a) Urban, J. J.; Talapin, D. V.; Shevchenko, E. V.; Murray, C. B. *J. Am. Chem. Soc.* **2006**, *128*, 3248. (b) Talapin, D. V.; Shevchenko, E. V.; Murray, C. B.; Titov, A. V.; Král, P. *Nano Lett.* **2007**, *7*, 1213.
(8) (a) Puntes, V. F.; Krishnan, K. M.; Alivisators, A. P. *Science* **2001**, *291*, 2115. (b) Sun, S.; Murray, C. B.; Weller, D.; Folks, L.; Moser, A. *Science* **2000**, *287*, 1989.
(9) (a) Fan, H.; Bentley, H. R.; Kathan, K. R.; Clem, P.; Lu, Y.; Brinker, C. J. *J. Non-Cryst. Solids* **2001**, *285*, 79. (b) Burkett, S.; Sims, S.; Mann, S. *Chem. Commun.* **1996**, *11*, 1367.
(10) (a) Lu, Y.; Fan, H.; Stump, A.; Ward, T. L.; Rieker, T.; Brinker, C. J. *Nature* **1999**, *398*, 223. (b) Fan, H.; Swol, F. V.; Lu, Y.; Brinker, C. J. *J. Non-Cryst. Solids* **2001**, *285*, 71.
(11) Caruso, F. *Adv. Mater.* **2001**, *13*, 11.
(12) Choi, S. Y.; Mamak, M.; von Freymann, G.; Chopra, N.; Ozin, G. A. *Nano Lett.* **2006**, *6*, 2456.
(13) Dai, Z.; Meiserb, F.; Möhwaldb, H. *J. Colloid Interface Sci.* **2005**, *288*, 298.
(14) Dinsmore, A. D.; Hsu, M. F.; Nikolaides, M. G.; Marquez, M.; Bausch, A. R.; Weitz, D. A. *Science* **2002**, *298*, 1006.

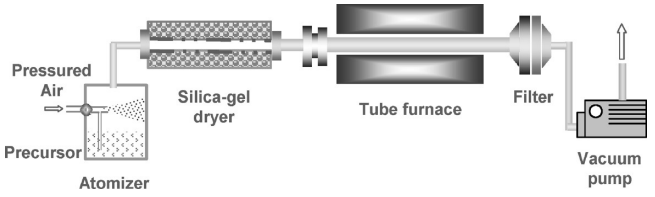

Figure 1. Schematic of the aerosol setup for the preparation of self-assembled mesospheres.

Experimental Section

Materials. Iron pentacarbonyl ($Fe(CO)_5$, 99.999%), oleic acid (99%), oleylamine (70%), 1-octadecene (ODE, ≥99.5%), heptane (99%), gold(III) chloride trihydrate ($HAuCl_4 \cdot 3H_2O$, ≥99.9%), chloroplatinic acid hexahydrate ($H_2PtCl_6 \cdot 6H_2O$, ≥37.5% Pt basis), and copper acetate ($Cu(CH_3COO)_2 \cdot 2H_2O$, 98%) were all purchased from Sigma-Aldrich. Electrostatically stabilized SiO_2 colloids of ST-40 (~15 nm, 40 wt %) and ST-20 L (~45 nm, 20 wt %) were obtained from Nissan Chemical America Corp. All the chemicals were used as received.

Syntheses of Fe_3O_4 and CuO Nanoparticle Dispersions. Oleic acid (6 mmol), oleylamine (3 mmol), and 1-octadecene (30 mL) were mixed and stirred in a three-neck flask under a gentle argon flow. Upon heating to 100 °C, $Fe(CO)_5$ (3 mmol, 0.588 g) was quickly syringe injected, and the solution turned from light yellow to dark brown instantly, indicating decomposition of $Fe(CO)_5$ into Fe followed by immediate oxidization. The mixture was allowed to reflux at ca. 280 °C for 60 min. Products were isolated and refined via a process of repeated precipitation in alcohol, centrifugation, and redispersion in heptanes and finally dispersed in 30 mL of heptane as a brownish-black suspension. For CuO, 80 mL of 0.02 M copper acetate aqueous solution was mixed with 0.5 mL of acetic acid and heated to 100 °C. Under vigorous stirring, 20 mL of 0.04 M NaOH solution was rapidly added into the boiling solution. Heating was removed until the mixture pH drops to around neutral. After cooling to room temperature, the product was subject to repeated centrifuging and washing and finally was dispersed in 100 mL of water as a dark brown suspension.

Aerosol Spray Drying/Pyrolysis. The aerosol system is illustrated in Figure 1. Aerosol droplets were created from a stainless steel pressure atomizer to generate, as measured by a laser aerosol spectrometer, geometric mean diameter ~1 μm droplets. Droplets were passed through a diffusion dryer to remove most of the solvent and then to a tube furnace to further densify the assembled particles or in some cases to thermally decompose precursor salts. Normal residence time is 1 s for the gas flow rate of 3.5 L/min used in most of the experiments. Product particles were collected on a 0.2 μm pore Millipore HTTP membrane filter (housed in a stainless steel holder covered by a heating tape to prevent recondensation of solvent vapor).

Fabrication of Fe_3O_4, SiO_2, and CuO Self-Assembled, Hollow-Structure, and Fe_3O_4/SiO_2 Hierarchical Assembled Mesospheres. For Fe_3O_4, 10 mL of as-synthesized Fe_3O_4/heptane dispersion was diluted by adding an additional 50 mL of heptane, aerosolized with argon carrier gas, and heated to 250 °C in the tube furnace or 450 °C for hollow structure. For SiO_2, 60 mL of 50 times diluted as-received 15 nm SiO_2 colloid (ST-40) was spray-dried with compressed air at 350 °C or 45 nm SiO_2 (ST-20 L) aqueous solution mixed with methanol at 1/4 v/v for the hollow structure. For CuO, 50 mL of as-synthesized CuO aqueous dispersion was directly spray-dried with compressed air at 350 °C. For the Fe_3O_4/SiO_2 hierarchical assembly, 0.125 mL (0.14 g) of as-received 15 nm SiO_2 colloid was dispersed in 20 mL of ethanol, 1.0 mL of Fe_3O_4/heptane was added into 39 mL of heptane, and then the two colloid systems were mixed and spray-dried (300 °C, Ar).

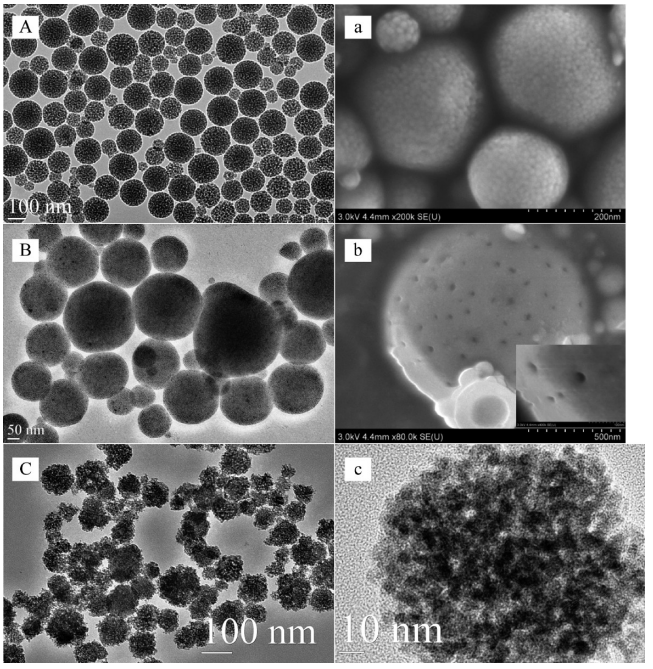

Figure 2. Electron images of self-assembled mesospheres of SiO_2 by TEM (A) and SEM (a), Fe_3O_4 by TEM (B) and SEM (b and inset), and CuO by TEM (C and c).

Characterizations. Morphologies and structures of prepared materials were examined by transmission electron microscopy (TEM, JEOL 2100 LaB6 and 2100F) and scanning electron microscopy (SEM, Hitachi SU-70). Analysis of elemental composition was performed by energy-dispersive X-ray spectroscopy (EDS) that is associated with the TEM. Phase identification was conducted by X-ray diffractometer (XRD, Bruker C2 Discover with GADDS), operating at 40 kV and 40 mA with unfiltered Cu Kα radiation (λ = 1.5406 Å). Real-time and in situ measurement of particle size distribution was carried out using a differential mobility analyzer (DMA, TSI Inc.) coupled with a condensation particle counter (CPC, TSI Inc.).

Results and Discussion

Iron oxide nanoparticle suspensions were synthesized via thermal decomposition of $Fe(CO)_5$ followed by spontaneous oxidation of Fe into Fe_3O_4 during the reflux process. As shown in Figure S1a in the Supporting Information, as-synthesized Fe_3O_4 nanoparticles exhibit a mean diameter of ca. 2.5 nm and arrange into well-ordered single or multilayers on the TEM grid. A high-resolution image (inset of Figure S1a) and selected area electron diffraction (SAED) pattern (Figure S1b) shows crystallinity and *d*-spacings, whose values are closer to those of magnetite Fe_3O_4 rather than γ-Fe_2O_3. Figures S2 and S3 show TEM images of as-received electrostatic-stabilized silica (~15 nm) and as-synthesized cupric oxide (~6 nm) nanoparticles, respectively.

Evaporation-driven assembling of Fe_3O_4, SiO_2, and CuO mesospheres were implemented via the aerosol route, and TEM and SEM results are shown in Figure 2. These images clearly show evidence of highly ordered packing particularly for the Fe_3O_4 and SiO_2 cases. Under an ideal case, a face-centered-cubic (fcc) or hexagonal close-packed (hcp) configuration (a packing factor of 0.74 for both[15]) of Fe_3O_4 or SiO_2 making a 100 nm sphere would contain roughly 5920 and 1754 primaries, respectively. For silica, which has larger primaries, the SEM resolution is sufficient to

(15) Schaffer, Saxena, Antolovich, Sanders, Warner *The Science and Design of Engineering Materials*, 2nd ed.; WCB/McGraw-Hill: New York, 1999.

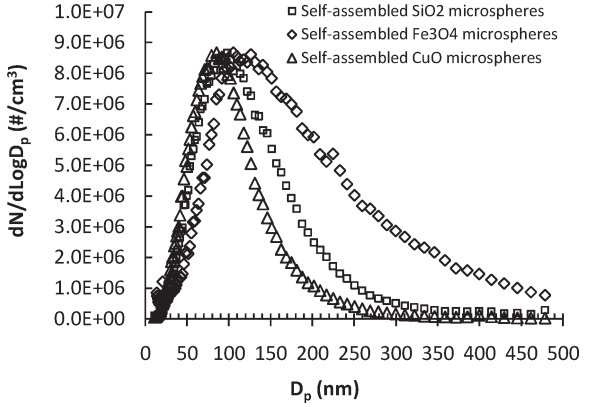

Figure 3. Size distributions of Fe_3O_4, SiO_2, and CuO self-assembled mesospheres measured by a differential mobility analyzer (DMA) coupled with a condensation particle counter (CPC).

show the surface packing of particles. This is not possible for Fe_3O_4, which has much smaller primaries. However, inspection of the SEM image (Figure 2b) indicates the nanoscale equivalent of "pinholes". We believe these are created to allow the internal heptane vapor to escape during the assembly because the very small primaries pack so closely, unlike the silica case. On the other hand, relative to Fe_3O_4 and SiO_2, self-assembled CuO mesospheres appear coarsely compacted (Figure 2C,c), which we believe can be attributed to the existence of some small chainlike or fractal clusters in the precursor suspension (see Figure S3).

Figure 3 shows the measured size distributions of the three different mesosphere materials. Both SiO_2 and CuO derived from aqueous dispersions exhibit relatively narrow size distributions with mean size of 100 nm. The size distribution of Fe_3O_4 is broadest, spanning over 250 nm, which can be attributed to the atomization process which is affected by surface tension, density, and other physical properties of the liquid medium, particularly the viscosity which changes as a result of different particle loadings.

The ability to make a dense packed structure as shown in Figure 2 implicitly requires that as the droplet evaporates and the surface concentration of nanoparticles increases, particles movement inward by diffusion and surface tension occurs at least as fast as the surface shrinkage as the droplet recedes. If, on the other hand, evaporation is sufficiently rapid, particles cannot move away from the receding surface, and their local density increases to the point that they begin to aggregate near the receding surface. Under such circumstances one should expect to see a hollow sphere composed of nanoparticles. To test this hypothesis, we performed an experiment using Fe_3O_4 under a faster solvent evaporation rate, by raising the furnace temperature from 250 to 450 °C. We observe the formation of hollow structured assembly of Fe_3O_4 as clearly seen in Figure 4A, in contrast to the compact structure (Figure 4a). Further confirmation of the hollow shell-like structure as appeared in Figure 4A was supported by the concentration profile of element Fe from EDS line scan characterization, which is shown in Figure S4. A further example was explored using a larger size, i.e., 45 nm, SiO_2 colloid (for decreasing particle diffusion) in a more volatile solvent of methanol (to enhance the evaporation) and shown in parts B and b of Figure 4 for the hollow and dense structure, respectively. The relative rates of these two competing processes occurring in a droplet are estimated for a quantitative comparison. Table 1 shows the calculated characteristic times for droplet evaporation and nanoparticle diffusion. It should be noted that the possible temperature variance of a droplet associated with the loss of

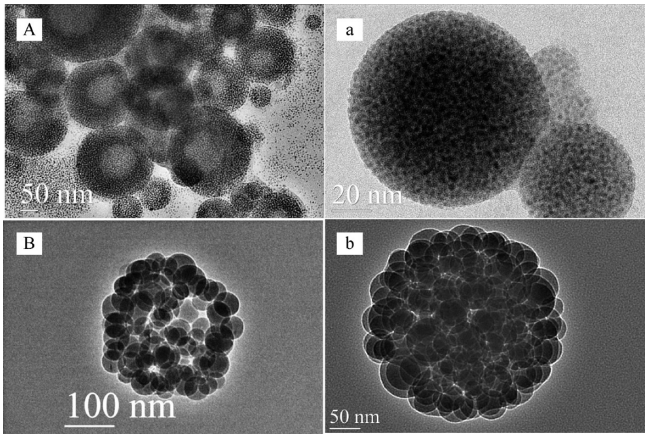

Figure 4. TEM images of hollow and compact structured Fe_3O_4 (A, a) and SiO_2 (B, b) assemblies.

Table 1. Comparison of Characteristic Times in Water and Heptanes (C_7H_{16}) Droplet Systems

system	T (°C)	evaporation t_e[a] (s)	diffusion t_d[b] (s)	t_e/t_d
SiO_2(15 nm)/H_2O	25	4.3×10^{-4}	7.7×10^{-6}	56
SiO_2(45 nm)/H_2O	25	4.3×10^{-4}	2.1×10^{-4}	2.1
SiO_2(45 nm)/CH_3OH	25	6.2×10^{-5}	1.2×10^{-4}	0.5
Fe_3O_4(2.5 nm)/C_7H_{16}	250	3.0×10^{-7}	7.9×10^{-9}	38
	450	6.3×10^{-8}	5.7×10^{-9}	11
Fe_3O_4(5.0 nm)/C_7H_{16}	450	6.3×10^{-8}	4.5×10^{-8}	1.4
Fe_3O_4(7.5 nm)/C_7H_{16}	450	6.3×10^{-8}	1.5×10^{-7}	0.4

[a] $t_e = (RT\rho_l d_l^2)/(8D_v M_l(p - p_\infty))$,[16] where R = universal constant, T = absolute temperature, ρ_l = density of the liquid phase, d_l = droplet diameter (approximated as the initial 1 μm mean size for calculations), D_v = diffusivity of solvent vapor in air, estimated by equation provided by EPA (http://www.epa.gov/athens/learn2model/part-two/onsite/est-diffusion-ext.html), M_l = molecular weight of liquid phase, p and p_∞ are partial pressures of solvent vapor on and far from the droplet, respectively. [b] $t_d = d_p^2/D_p = 3\pi\eta d_p^3/k_B T$,[17] where d_p = particle diameter, D_p = diffusivity of particle in liquid phase, η = viscosity of liquid phase, and k_B = Boltzmann's constant. Change in vapor pressure due to a curved liquid/vapor interface (meniscus) of droplet is trivial as estimated from the Kelvin equation and therefore was not counted.

vaporization heat during the evaporation process was not considerate in this simplistic model.

For the SiO_2 (15 nm)/H_2O system, Table 1 shows that the evaporation time is 50 times higher than the diffusion time even at room temperature, suggesting the slow evaporation condition and resultantly a compact structure which is consistent with Figure 2A,a. For the larger 45 nm SiO_2 system, the time ratio of t_e/t_d crosses over the unity from 2.1 to 0.5, when switching solvent from water to methanol. This is reasonably matched to the change in particle morphology as seen in Figure 4B,b. With the substitution of methanol for water, although diffusion is enhanced (from 2.1×10^{-4} to 1.2×10^{-4} of t_d) due to the decrease of solvent viscosity, evaporation is even more intensified (from 4.3×10^{-4} to 6.2×10^{-5} of t_e) due to the increase of the solvent vapor pressure.

Unlike water, the nonpolar heptane (C_7H_{16}) in the Fe_3O_4/heptane system does not appreciably evaporate in the diffusion dryer filled with silica gel. Thus, heptane drying has to occur primarily in the tubular furnace. Comparing the two characteristic times of Fe_3O_4(2.5 nm) particles in C_7H_{16} at 250 and 450 °C,

(16) Kim, S. H.; Liu, B. Y. H.; Zachariah, M. R. *Chem. Mater.* **2002**, *14*, 2889.
(17) Seinfeld, J. H.; Pandis, S. N. *Atmospheric Chemistry and Physics*; John Wiley & Sons: New York, 1998.

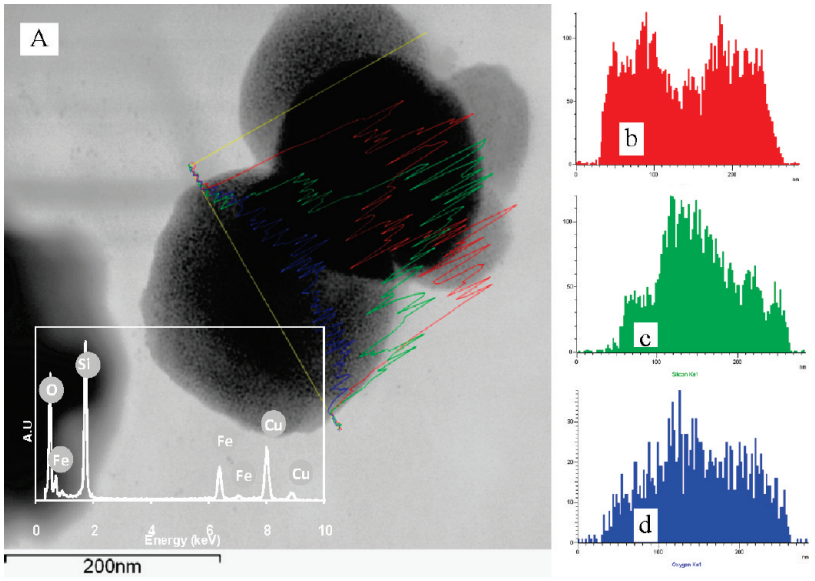

Figure 5. EDS area and line scan analysis of a single hierarchical-assembled Fe_3O_4/SiO_2 composite particle (A), revealing elemental concentration profile of Fe (b), Si (c), and O (d) across the line, and on the whole particle area (inset of (A)).

Table 1 demonstrates that as temperature increases, the evaporation time decreases much faster than the diffusion time does. At 250 °C, the ratio of t_e/t_d is 38 ($\gg$1), suggesting the formation of compact Fe_3O_4, which is indeed confirmed by Figure 4a (a high-resolution image of sample same as that is shown in Figure 2b). This ratio drops to 11, a value that would still suggest a compact structure, although the TEM images clearly show a hollow material. This discrepancy indicates that we have neglected the fact that aggregates do form during the assembly process and that their transport properties are not accounted for in this simple-minded model. To at least address this point, we approximate the effect of aggregation by using 5 and 7.5 nm of aggregate size in the calculations as listed in the table, and the derived values of the characteristic time ratio indicate indeed that the larger aggregate size, the more favorable formation of a hollow structure becomes.

Finally, we turn to the issue of two component assembly. Because of surface dissimilarity between oleic acid-capped Fe_3O_4 (hydrophobic and neutral) and electro-stabilized SiO_2 (hydrophilic and negatively charged), a general solution-phase route cannot homogenize the two systems without further surface modification. For example, Hodgkins et al. conducted hydrophilic surface functionalization of maghemite nanocrystals with thiol organosiloxane groups before they could introduce them into SBA-15 type mesoporous silica.[18] On the other hand, macroscopic phase separation can be circumvented in the aerosol approach so long as an intermiscible hybrid solvent system is available. In our case this turned to be a heptane−water−ethanol trisolvent system. After being aerosolized, phase separation and homogeneous self-assembly occur in the microscopic droplet during the course of differential solvent evaporation. Self-assembly of SiO_2 should occur first in the diffusion dryer, which would presumably result in a core particle of assembled silica. As the droplet is heated, evaporation of heptane will precipitate Fe_3O_4 on the exterior surface of the silica to yield a core−shell like structure. Careful examination of the TEM image (Figure 5A) reveals that indeed the outside of the particle has very fine structures, which are consistent with the iron oxide. EDS line scan analysis of a single composite particle reveals elemental concentration profile of Fe (Figure 5b), Si (Figure 5c), and O (Figure 5d), confirming the core−shell like structure. Energy-dispersive spectroscopy (inset of Figure 5A, signal of element C coming from coating on copper grid is not included) of the whole particle area was collected as well. The presence of both Fe and Si was clearly identified, and a Si/Fe atomic ratio equivalent to 5.22 was quantified, correlating reasonably well with the initial mixing ratio of 4.75.[19] This corresponds to an approximate particle number ratio Fe_3O_4 (2.5 nm)/SiO_2 (15 nm) of 23.1. The relatively irregular shape of the particles, as compared to the pure iron oxide or silica systems, would seem to suggest that some internal mixing of the particles, presumably trapping iron oxide within the silica core, resulted in a nonspherical shape.

The X-ray diffraction patterns with representative index on typical peaks are given in Figure S5. Patterns of (a), (b), (c), and (d) correspond to self-assembled SiO_2, Fe_3O_4, hierarchical-texture Fe_3O_4/SiO_2, and self-assembled CuO mesospheres, respectively; the diffraction peaks index to crystalline cubic Fe_3O_4 (JCPDS 19-0629) and CuO (JCPDS 41-0254).

Conclusions

In summary, one- or bicomponent assemblies of nanospheres have been realized through an aerosol approach. Structure control of the self-assembly was achieved through simply adjustment of solvent evaporation rates. This approach should be generic to any nanoparticle system of mixture.

Acknowledgment. The authors gratefully acknowledge the financial support of the NSF and the DOE-BES and acknowledge microscopy support of the Maryland NanoCenter and the NSF-UMERC.

Supporting Information Available: TEM images of as-received silica colloid, as-synthesized iron oxide and cupric oxide nanoparticles, and XRD patterns of the reported materials. This material is available free of charge via the Internet at http://pubs.acs.org.

(18) Hodgkins, R. P.; Ahniyaz, A.; Parekh, K.; Belova, L. M.; Bergström, L. *Langmuir* **2007**, *23*, 8838.

(19) A Si/Fe atomic ratio of 4.75 is based on 100% Fe_3O_4 yield after synthesis and purification; if, for example, the accumulated yield is 50%, the actual Si/Fe mixing ratio will be 9.5. We assume it rational when the quotient of the two ratios from EDS and initial mixing is within a scope of 1 order of magnitude.